International Journal of Signal Processing, Image Processing and Pattern Recognition
Vol.9, No.6 (2016), pp.215-226
http://dx.doi.org/10.14257/ijsip.2016.9.6.19

Local Image Matrix Based on Poynting Vector and Its Application in RTM

Yang Hongyu[1] and Liu Jicheng[2]

[1] *Northeast Petroleum University, Daqing,Heilongjiang,China, 163318*
[1]*yanghongyu1971@126.com*, [2]*ljcdqpi@163.com*

Abstract

Poynting vector is used to decompose source and receiver wavefields into different angle, then the partial images of different incident and scatter angle are computed and local imaging matrix(LIM) can be constructed. LIM composes all the angle information which is related with the geological structure, and it can be used as the base of angle-domain imaging analysis. We used LIM to reverse time migration image in angle domain and geological dip estimate. The numerical example is tested to demonstrate the computation method.

Keywords*: Local Image Matrices (LIM), Reverse Time Migration(RTM), Low Frequency Artifacts, Dip Estimation*

1. Introduction

Seismic migration can not only image for geological structure, but also be applied to the attribute analysis such as velocity updating and AVA. There are two kings of Pre-stack depth migration: ray-based and wave equation based migration methods. Ray-based methods are established on high frequency asymptotic approximation, which can't handle the wave phenomenon such as scatter, diffraction *etc.*, especially it isn't fitted for strong transverse velocity change, although as its high computation efficiency. Wave-equation based migration includes one-way and full-way migration methods. One-way propagator only can model wavefields in limited propagation angle and can't handle turning wave, so the complicated structure such as steep and overlapped structure can't be imaged correctly. Full-wave equation based RTM(Reverse Time Migration) propagates waves in all directions without any angle limitation and images steep structures with dip angles up to 180°, giving it advantages over other migration methods [1-4].

Angle domain image evokes research interest because seismic illumination analysis, image resolution and image correction and image gather extraction can be conducted through analyzing the interaction between incident and reflection in angle domain [5-7]. The critical step in angle domain is to compute the propagating direction of wavefields. As the solution of wave eqation can't give the propagation direction directly, the propagating direction need to be extracted. There are mainly three kinds of methods to extract the angle information. The first is vector-based method, including Poynting vector[8], polarization vector and transient wave-number [9-11]. This kind of methods computes the normal direction of wave-front to express the propagating direction and have higher computation efficiency, but only one propagating direction can be obtained at every image point and one time step, which maybe unstable for complicated wave-field. The second kind of methods is local-plane-wave decomposition[12-15], which decomposes local wavefields by using FFT, wavelet and slowness, then the information of wavefields is converted into slowness domain or wave-number domain and the wave propagating direction is extracted. This kind of method is stable compared with the first kind of methods, but need expensive computation. The last kind of methods is local-shift image condition method [16-20], which computes the image with time or space shift to

ISSN: 2005-4254 IJSIP

extract wave propagating direction during imaging process. The method also has quickly computation speed, but exists smearing effect and is difficult to compute for 3D model.

LIM(Local Image Matrix) is introduced in the paper which was proposed in [5].Poynting vector is used to decompose the source and receiver wavefields along different direction, then partial image is computed for different incident and scattering angle combination, so LIM can be constructed. LIM contains all the angle information among wave propagating and geological structure interaction during imaging, including incident angle, scattering angle, dip, and reflection angle, ect.. The matrix can be used as the base for image analysis in angle domain. Summation of partial image in LIM is depth image. Different gathers can also be extracted by summation partial image according to different parameters, such as common reflection gathers, common dip gathers, which can be used to velocity analysis, AVA, illumination analysis and noise filtering. We use LIM to remove artifact during RTM and estimate dip. Simple model and SEG Salt model are conducted to demonstrate this method.

2. Wavefields Decomposition

Conventional zero-lag cross-correlation between source and receiver wavefields is as follows[21]:

$$I(\mathbf{r}) = \int_0^{T_{\max}} u_S(\mathbf{r},t) \cdot u_g(\mathbf{r}, T_{\max} - t)\, dt \tag{1}$$

Where $u_S(\mathbf{r},t)$ and $u_g(\mathbf{r},t)$ are source and receiver wavefields repectively at time t and space $\mathbf{r} = (x, y, z)$, $T_{\max}$ is the total recording time. Propagation direction θ is introduced into source and receiver wavefields, then we can get $u_S(\theta_S, \mathbf{r}, t)$ and $u_g(\theta_g, \mathbf{r}, t)$,which are used to image condition(1), the partial image in angle domain is[5]

$$I(\theta_s, \theta_g, \mathbf{r}) = \int_0^{T_{\max}} u_s(\theta_s, \mathbf{r}, t) \cdot u_g(\theta_g, \mathbf{r}, T_{\max} - t)\, dt \tag{2}$$

Where θ_s and θ_g is incident angle and scattering angle of source and receiver wavefields. We can transform the observation coordinate （θ_s， θ_g） to target coordinate （θ_r， θ_d）. The relation is shown as Figure 1, where n_r is the normal direction of reflector, θ_r is the reflection angle relating to normal and θ_d is the dip of reflector. Summing up all partial images $I(\theta_s, \theta_g, \mathbf{r})$, the final image is

$$I(\mathbf{r}) = \sum_{\theta_s} \sum_{\theta_g} I(\theta_s, \theta_g, \mathbf{r}) \tag{3}$$

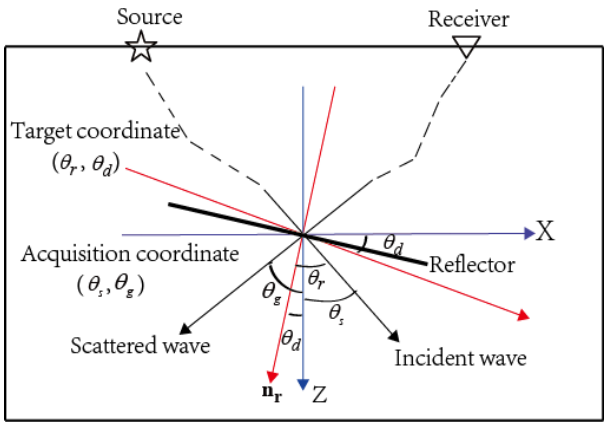

Figure 1. Observation Coordinate (Blue) and Target Coordinate (Red)

The important problem in angle domain is how to extract the propagation direction. The angle information isn't shown explicitly in wave equation solution. Poynting vector based method to compute the direction has high efficiency and is used widely although there maybe unstable for complicated wavefields. Many authors propose different methods to improve the stability, Yoon ect. adopt Gaussian-weighted function in time domain to improve the stability of Poynting vector [22], zhang ect. use smoothed velocity model and smooth wavefields to improve direction stability [23], Thomas ect. smooth Poynting vector in space domain to obtain stable angle estimation [24]. Yoon and Marfurt adopt the product of space gradient and time derivation of wavefields to compute Poynting vector, which has complicated computation and results maybe unstable as needing to compute time derivation and space gradient of wavefields. For 2D acoustic wave equation, its single order stress-velocity equation is

$$\begin{cases} \dfrac{\partial u}{\partial t} = \rho v^2 \left(\dfrac{\partial v}{\partial x} + \dfrac{\partial w}{\partial z}\right) \\ \dfrac{\partial v}{\partial t} = \dfrac{1}{\rho}\dfrac{\partial u}{\partial x} \\ \dfrac{\partial w}{\partial t} = \dfrac{1}{\rho}\dfrac{\partial u}{\partial z} \end{cases} \tag{4}$$

Where v is velocity, u is wavefields, ρ is medium density, v and w is vibration velocity of x and z direction respectively. Then Poynting vector can be calculated by the product of stress and particle velocity[25]:

$$\vec{P} = -\mathbf{v} \cdot \nabla u \tag{5}$$

Where $\mathbf{v} = (v, w)$ is velocity vector. Space gradient of u and velocity w and v are the intermediate calculation results when using staggered grid to construct wavefields propagator. So Poynting vector can be computed easily. Figure 2 is the snapshots of source wavefields Poynting vector for a simple two layers model, where the propagation direction can be determined. Figure 2(a) is horizontal component, white and black express right and left direction respectively. Figure 2(b) is vertical component, white and black express downward and upward direction.

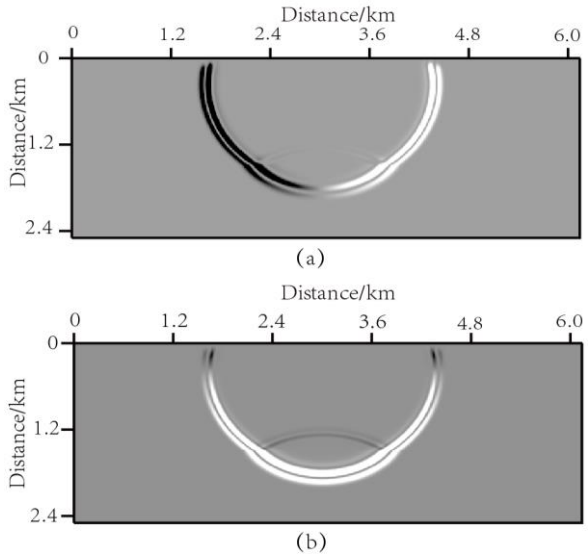

Figure 2. Snapshots of Poynting Vector
(a) Horizontal Component (b) Vertical Component

According to Poynting vectors, the propagation direction of wavefields is

$$\theta = \arctan\left(\frac{p_x}{p_z}\right) \tag{6}$$

Where p_x, p_z is horizontal and vertical components of Poynting vector.

3. Local Image Matrix

LIM is the expansion of the conventional image condition. It is a function of the incidence-scattering angle pairs at the target reflector[15]

$$I(\theta_s, \theta_g, \mathbf{r}, t) = \int_{A_s}\int_{A_g} u_s(\theta_s, \mathbf{r}, \mathbf{r}_s, t) \cdot u_g(\theta_g, \mathbf{r}, \mathbf{r}_g, T_{\max} - t) d\mathbf{r}_s d\mathbf{r}_g \tag{7}$$

Where θ_s is the local incident angle, θ_g is the local scattering angle, $u_s(\theta_s, \mathbf{r}, \mathbf{r}_s, t)$ is local incident wave at source $\mathbf{r}_s$, $u_g(\theta_g, \mathbf{r}, \mathbf{r}_g, t)$ is local scattering wave at receiver $\mathbf{r}_g$, A_s and A_g is the apertures of source and receiver arrays, respectively. The inner integral sums up the contributions from all the receivers for the same source to a scattered beamlet at θ_g, the outer integral sums contributions from different sources. Applying the image condition to local incident wave with angle θ_s and local scattering wave with angle θ_g, and stacking them result in a partial image in local angle domain (θ_s, θ_g). LIM is composed of all the partial images. The final image in the space domain comes from LIM by summing up the contributions of all scattering events (θ_s, θ_g). According to figure 1, the local angle coordinate constructed by observation coordinate (θ_s, θ_g) can be transformed to target coordinate (θ_r, θ_d)

$$\begin{aligned} \theta_s + \theta_g &= 2\theta_d \\ \theta_s - \theta_g &= 2\theta_r \end{aligned} \tag{8}$$

So formula (3) can also be transformed to

$$I(\mathbf{r}) = \sum_{\theta_s} \sum_{\theta_g} I(\theta_s, \theta_g, \mathbf{r}) = \sum_{\theta_r} \sum_{\theta_d} I(\theta_r, \theta_d, \mathbf{r}) \tag{9}$$

Figure 3 shows the feature of the local image matrixes for two typical reflectors. The left panels are velocity models of different reflectors, and the right are LIM of the points in model grid. The horizontal and vertical axes are incident and scattering angles. For a local horizontal reflector, the energy is concentrated at the diagonal of the matrix, which meets the reflection principle, *i.e.*, incident angle equals to the reflection angle. For a dipping reflector, the energy still forms a strip parallel to the diagonal but shifts for a distance, which shows the dip of the imaging point. So LIM can describe all the angle information formed by the interaction of wave and geological structure during imaging in angle domain, which is the imaging analysis basis in angle domain. According to (8), LIM can be expressed the function of reflection angle and dip as shown in figure 4. The horizontal and vertical axes denote incident and scattering angles respectively, the main diagonal (from upper-left to lower-right) describes the reflection angles θ_r, the energy distribution along the diagonal gives angle related information that can be used in velocity updating, AVA analysis *etc.* The side diagonal(from upper-right to lower-left) corresponds to dip θ_d,The offset of the energy measured along the diagonal direction carries the dipping information of the structure. The offset from main diagonal expresses the value of dip. Otherwise, different image gathers may also be constructed from LIM, For example, integrating the energy along the horizontal direction gives the common scattering angle gather, and summing up the energy along the vertical direction gives the common illumination angle gather, *etc.* LIM reveals many characteristics such as velocity model, reflect performance, illumination analysis *etc.*. Some operations such as noise removal, dip measurement, gather extraction can be performed in LIM.

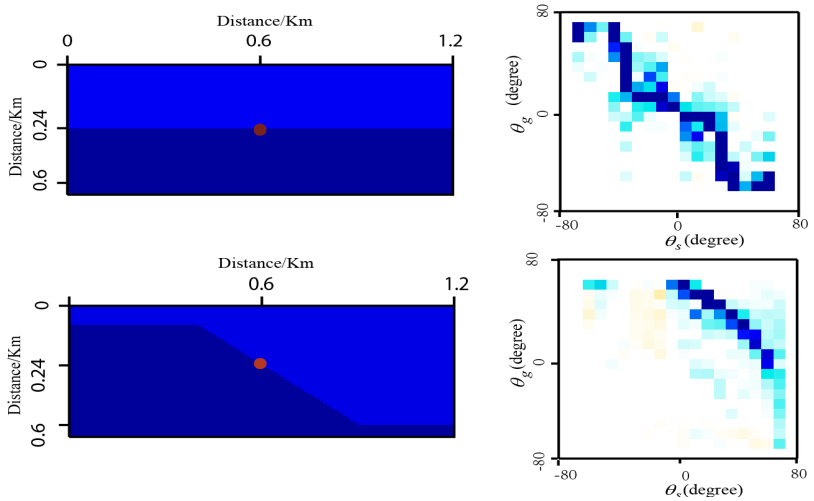

Figure 3. The Local Image Matrixes for Typical Structures

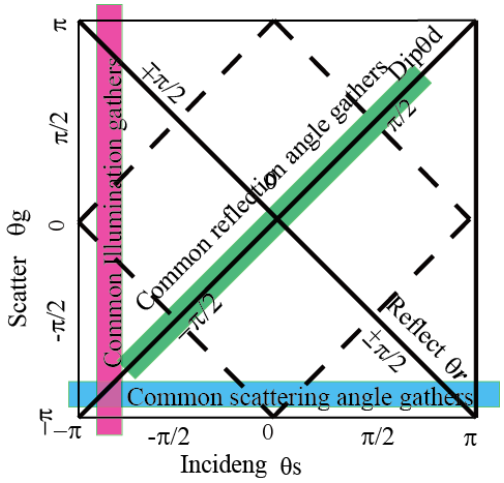

Figure 4. The Local Image Matrix

4. Low Wave-Number Noise Removal and Dip Measurement

4.1. Low Wave-Number Noise Removal

According to the correlation image condition, image is formed not only at reflector, but also at the non-reflector along the propagating path, which produces low-number noise in RTM. Esteban D´ıaz and Paul Sava analyze the low wave-number noise mechanism and the kinematic synchronization between source and receiver wavefields reconstructed in the subsurface [26].

There are mainly three kinds of method proposed to remove low wave-number noise in industry. The first is to modify wave equation. Baysal *etc.* use non-reflection equation to eliminate inner reflection in the vertical incident wave, but it is only suitable to post-stack data [27]. Loewenthal *etc.* improve Baysal's method, he uses a window whose length is wider than wavelength to smooth velocity model to eliminate inner reflection, the method has better effect but it also eliminates useful information and influence the image quality[28]. The second class is to remove noise during imaging. Kwang Jin and Yoon ect. apply Poynting vector to image condition and obtained better effect [29]. Faqi Liu ect. decompose wavefields into upward/downward wave and leftward/rightward wave, then only the opposite direction wavefields components are retained when using image condition and noise is removed effectively[30]. Yan and Xie propose a plane wave decompose in slowness domain to decompose wavefields and obtained better effect, but FFT is needed and has higher computation [15]. Sava ect. use local time or space offset and Randon transform to compute wave propagating direction and it also need huge computation [16-20]. The last class methods is to filter post-stack image. Antoine Guitton ect. adopt the prediction error filter to remove noise. Zhang ect. point out that Laplacian operator filter is equivalent to image wavefields attenuation in angle domain and needn't to output angle gathers [31]. Poynting vector method has very high computation efficiency, so we use it to decompose wavefields and filtered low-number noise in angle domain.

Figure 5(a) is conventional correlation image for a simple two layers model. The constant velocity model used for prestack migration is 512 points in x-direction and 208 points in z-direction. The interval of x-direction and z direction are 12 m. The upper layer velocity is 2.8Km/s and bottom layer velocity is 3.9Km/s. A 15 Hz wavelet is used for calculating synthetic data set. The geometry is dual-side 250 receivers with 24m interval. The interval of shots is 60 m and the number of shots is 100. Figure 5(c) is LIM for a location in (a), the location is not a reflector so strong low wave-number noise exists

because of the backscattering wave of source and receiver. It can be seen obviously that energy mainly distributes at near ±90° reflection angle, which describes clearly the mechanism of low wave-number noise. If a angle domain filter is designed to attenuate events with very wide reflection angles, then low wave-number noise can be removed effectively. Figure 5(c) is the image that filtered in angle domain with formula (10). The low wave-number noise in shallow layer is removed significantly and image quality is improved obviously.

$$F(\theta_r, \theta_d) = \begin{cases} 1 & \theta_r \le 60^0 \\ 0 & \theta_r > 60^0 \end{cases} \tag{10}$$

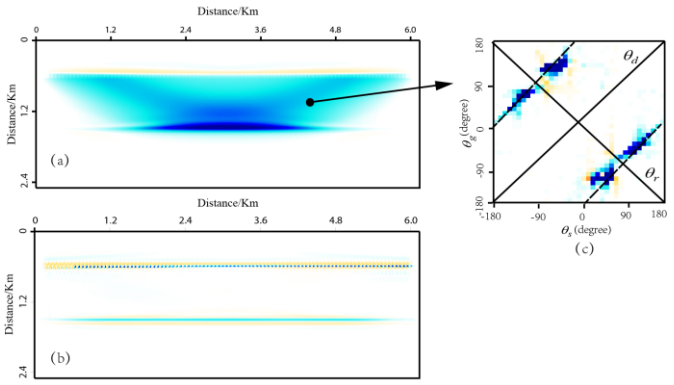

Figure 5. A Simple Example for LIM used to Remove Artifacts

We apply the analysis method to the SEG Salt model. Figure 6(a) is the velocity model with 1300 points in x-direction and 300 points in z-direction. The interval of x-direction and z direction are 10.16 m. The synthetic data set is modeled using 126 surface sources with interval of 101.6 m. The source time function is a 15-Hz Ricker wavelet. 1260 receivers are used and the interval is 10.16m. The Differential equation is 2th order in time and 4th order in space staggered format, PML absorbing boundary condition is applied. Poynting vector is calculated by (5) and angle computation is as (7). Figure 6(b) is conventional cross-correlation image, and Figure 6(c) is the image filtered in angle domain by using (9). Comparing 6(b) and (c),the strong noise covers the true image in conventional image, especially in shallow of model, which is difficult to distinguish the correct image. After filtered in angle domain, low-number noise is removed effectively and the reflectors are also retained very well.

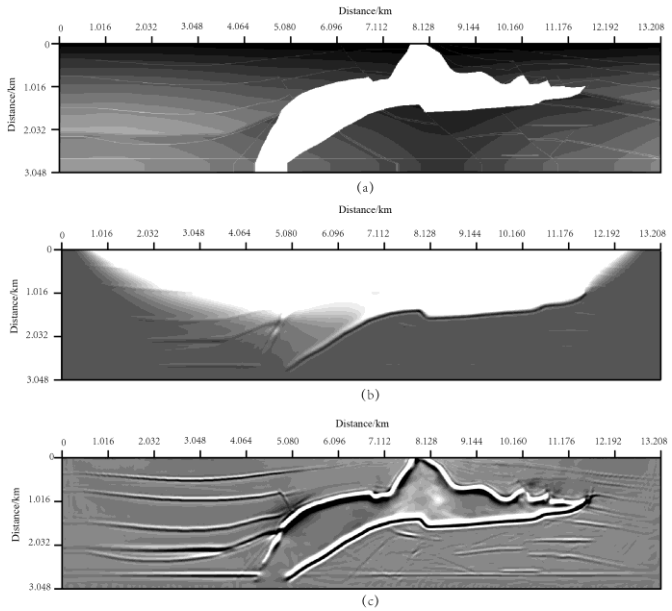

Figure 6. Migration for SEG/EDAGE Model
(a) Velocity Model; (b) Conventional Image; (c) Image in Angle Domain

4.2. Dip Estimate

We can construct common dip gathers to estimate geological dip quantitatively. In Figure 4, summing up energy along the upper-left to lower-right direction, the energy distribution along upper-right to lower-left direction gives the information about reflector dips. Figure 7 is a simple five layers model and the velocity of every layer is indicated. The grid is 512 points in x-direction and 208 points in z-direction. The interval of x-direction and z direction are 12 m. The number of shots is 301 and interval of shots is 48m. The geometry is dual-side 250 receivers with 24m interval. We overlapped the model and common dip gather to demonstrate dip measurement. The dip of reflector at location 1 and 4 is zero, so all energy peaks are centered at diagonals. The first reflector at location 2 and 3 is flat but followed by three reflectors with increasing dipping angles. The shift of energy peaks from the center lines reveals their dip angles which can be quantitatively measured.

We also test the dip estimate for complicate model *i.e.* SEG Salt model. The result is shown as Figure 8. Ten locations were selected to estimate the corresponding structure dip, as shown in the top figure. Because the physical characteristic of the high velocity salt, the wavefields above salt are very complicated, and the Poynting vectors are unstable as discussed before, which leads to more noise when computing dip. But the lower salt boundary dip can be clearly shown, the enlarged portion shows the details of the result. The lower salt boundary dips toward the left with a pretty steep angle. The base line is horizontal. Other reflectors are toward the right with mild dip angles. All these features are clearly shown and angles can be quantitatively estimated using their shifts.

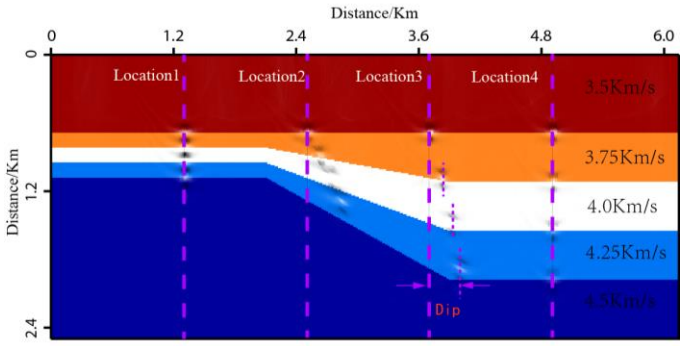

Figure 7. Dip Estimate for a Five Layers Model

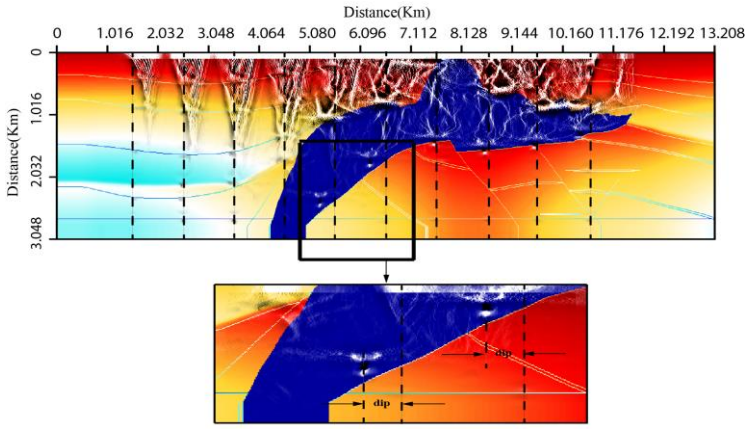

Figure 8. Dip Estimate for SEG Model

5. Conclusion

An approach using Poynting vector for extracting angle domain information from migrated wavefields is proposed in the paper. We construct local image matrix based Poynting vector. LIM provides much useful information about the subsurface reflectors. Properly sorting the energy within LIM, we remove artifacts and estimate dip of reflectors. According to the method discussed, numerical computation results for some simple models and SEG salt model are demonstrated and the results show the effectiveness of the method.

Acknowledgments

The paper is supported by Nature Science Fund of Heilongjiang Province,China(NO.2014F04).We thank for the Xie X.B. providing much suggestion and some original codes when J.C. Liu was visiting at his Lab.. Chen Bo and Luo J.R. also gave helpful discussions.

References

[1] C. Hemon, "Equations d''onde et models. Geophysical Prospecting, vol. 26, **(1978)**, pp. 790-821.
[2] Baysal, E., D. K. Dan, and W. John. Reverse time migration. Geophysics, vol. 48, **(1983)**, pp. 1514-1524.
[3] L.Dan and R.M. Irshad, "Reverse time migration in spatial frequency domain", Geophysics, vol. 48, **(1983)**, pp. 627-635.
[4] T. Chen and L. J. Huang, "Imaging Steeply-Dipping Fault Zones Using Elastic Reverse-Time Migration with a Combined Wavefield-Separation and Poynting-Vector Imaging Condition",Thirty-Ninth Workshop on Geothermal Reservoir Engineering, Stanford, California,**(2014)** February 24-26, pp. 1-11.
[5] X. B. Xie and R. S. Wu, "Extracting angle domain information from migrated wavefields", 72th Annual International Meeting, SEG Expanded Abstracts, Salt Lake City, Utah, **(2002)** October 6-11, pp. 1360–1363.
[6] X. B. Xie and R. S. Wu, "A depth migration method based on the full-wave reverse-time calculation and local one-way propagation", 76th Annual International Meeting, SEG Expanded Abstrac, New Orleans, **(2006)**, pp. 2333-2337.
[7] X. B. Xie, Y. Q. He and P. M Li, "Seismic illumination analysis and its applications in seismic survey design", Chinese Journal of Geophysic.(in Chinese), vol. 5, **(2013)**, pp. 1568-1581.
[8] K. Yoon and K. J. Marfurt, "Reverse-time migration using the Poynting vector: Exploration Geophysics", vol. 37,**(2006)**, pp. 102–107.
[9] Q. Zhang and G. A. McMechan, "Common-image gathers in the incident phase-angle domain from reverse time migration in 2D elastic VTI media", Geophysics, vol. 6, no. 76, **(2011)**, pp. S197–S206.
[10] Q. Zhang and G. A. McMechan, "2-D and 3-D elastic wavefield vector decomposition in the wavenumber domain for VTI media", Geophysics, vol. 3, no. 75,**(2010)**, pp. 13–26.
[11] Q. Zhang and G. A. McMechan, "Direct vector-field method to obtain angle-domain common-image gathers from isotropic acoustic and elastic reverse-time migration", Geophysics, vol. 5, no. 76, **(2011)**, pp .WB135–WB149.
[12] R. Yan and X. Xie, "A new angle-domain imaging condition for reverse time migration: 79th Annual International Meeting, SEG, Expanded Abstracts, Houston, **(2009)**, pp. 2784–2788.
[13] R. Yan and X. Xie, "A new angle-domain imaging condition for elastic reverse time migration: 80th Annual International Meeting, SEG, Expanded Abstracts Denver, **(2010)**, pp. 3181–3186.
[14] R. Yan and X. Xie, "Angle gather extraction for acoustic and isotropicelastic RTM: 81st Annual International Meeting, SEG, Expanded , San Antonio, **(2011)**, pp. 3141–3146.
[15] R. Yan and X. Xie, "An angle-domain imaging condition for elastic reverse time migration and its application to angle gather extraction", Geophysics, vol. 5, no. 77, **(2012)**, pp. S105–S115.
[16] P. Sava and S. Fomel, "Angle-domain common-image gathers by wavefield continuation methods: Geophysics, vol. 68, **(2003)**, pp.1065–1074.
[17] P. Sava and S. Fomel, "Coordinate-independent angle-gathers for wave equation migration: 75th Annual International Meeting, SEG, Expanded Abstracts, Huston. **(2005)**, pp 2052–2055.
[18] P. Sava and S. Fomel, "Wave equation common-angle gathers for converted wave: 75th Annual International Meeting, SEG, Expanded Abstracts, Huston. **(2005)**, pp. 947–951.
[19] P. Sava and S. Fomel, "Time-shift imaging condition for converted waves: 76th Annual International Meeting, SEG, Expanded Abstracts, New Orleans, **(2006)**, pp. 2460–2464.
[20] P. Sava and S. Fomel, "Time-shift imaging condition in seismic migration:Geophysics, vol. 6, no. 71,**(2006)**, pp. S209–S217.
[21] J. F. Claerbout, "Imaging the Earth's Interior", Blackwell Scientific Publications,**(1985).**
[22] Yoon, K., M. Guo, J. Cai, and B. Wang, "3D RTM angle gathers from source wave propagation direction and dip of reflector", 81st Annual International Meeting, SEG, Expanded Abstracts, San Antonio, **(2011)**, pp. 3136–3140.
[23] Q. Zhang an G. A. McMechan, "Common-image gathers in the incident phase-angle domain from reverse time migration in 2D elastic VTI media", Geophysics, vol. 76, **(2011)**, pp. 197–206.
[24] A. D. Thomas and Q.W. Graham, "RTM angle gathers using Poynting vectors", 81th Annual Meeting, SEG Expanded Abstracts, San Antonio, **(2011)**, pp. 3109-3113.
[25] K.Yoon, Marfurt and W. Starr, "Challenges in reverse-time migration", 74th Annual International Meeting, SEG Expanded Abstracts, Denver, Colorado, **(2004)** October 10-15, pp. 1057–1060.
[26] E. D´ıaz and P. Sava, "Understanding the reverse time migration backscattering: Noise or signal?", CWP-712, pp.111-125.
[27] E. Baysal, D. D. Kosloff and J.W.C. Sherwood, "A two way nonreflecting wave equation", Geophysics, 49, **(1984)**, pp. 132-141.
[28] D. Leowenthal, P. A. Stoffa and E. L. Faria, "Suppressing the unwanted reflections of the full way equation", Geophysics, vol. 52, **(1987)**, pp. 1007-1012.
[29] Y. K. Jin, K. J. Marfurt and W. Starr, "Challenges in reverse time migration", 74th Annual International Meeting,SEG Expanded Abstract, Denver, Colorado, **(2004)** October 10-15, pp. 1057–1060.
[30] L. Faqi, Z. Guanquan, S. A. Morton, "Reverse-time migration using one-way wavefield imaging condition 77th Annual International Meeting,SEG,Expanded Abstract,vol. 1, no. 26, **(2007)**, pp. 2170-2174.

[31] Z. Yu and J. Sun, "Practical issues of reverse time migration: true amplitude gathers,noise removal and harmonic-source encoding", CPS/SEG International Geophysical Conference & Exposition,**(2009)**, Beijing .

Authors

Yang HongYu is a doctor candidate of Northeast Petroleum University, China. His research interests include Oil&Gas information processing.

Jicheng Liu is a full professor in the school of computer in School of Electrical and Information Engineering, University of Northeast Petroleum, China. He obtained his PhD degree from Beihang University(BUAA),China, 2003.His research interests mainly include non-stationary signal processing and seismic signal processing.